Available online at www.sciencedirect.com
SCIENCE DIRECT
Journal of Catalysis 238 (2006) 412–424
JOURNAL OF CATALYSIS
www.elsevier.com/locate/jcat

Novel Ni catalysts for methane decomposition to hydrogen and carbon nanofibers

Yong Li, Baocai Zhang, Xiaowei Xie, Junlong Liu, Yide Xu, Wenjie Shen *

State Key Laboratory of Catalysis, Dalian Institute of Chemical Physics, Chinese Academy of Sciences, Dalian 116023, China

Received 11 November 2005; revised 20 December 2005; accepted 24 December 2005

Available online 27 January 2006

Abstract

Novel nickel oxides with controlled crystalline size and fibrous shape were successfully prepared by precipitation of nickel acetate and sodium carbonate aqueous solution with the mediation of ethylene glycol. The precipitation media and temperature were found to play crucial roles in determining the crystalline size and shape of the nickel oxides. The NiO prepared in the aqueous solutions exhibited mainly spherical particles with few nanorods, whereas the NiO samples prepared in the solution of ethylene glycol could be of spherical, fibrous, or nanorod shape, depending on the precipitation temperature. In particular, the nickel hydroxide precipitate obtained in the solution of ethylene glycol at 393 K was α-$Ni(OH)_2$ with hydrotalcite-like structures; further calcination of this precipitate at 573–1073 K resulted in the formation of nickel oxides with similar fibrous shapes and crystalline size of 3.0–8.1 nm. Similar metallic Ni crystalline size of about 11 nm and fibrous structure were obtained by reduction of these NiO samples with hydrogen at 773 K. When further exposed to the reaction of methane decomposition, the metallic Ni crystallines still exhibited similar evolution behavior and rapidly stabilized at the critical size of 17–18 nm. Consequently, very close catalytic activities for methane decomposition over these novel Ni catalysts were observed with the carbon yields of 354–398 g_C/g_{Ni}. The Ni crystallines departed from the fibrous structures and gradually aggregated into particles by the dissociation of the deposited carbons. These nickel particles were then highly dispersed on the in situ produced carbon, which can inhibit the further growth of nickel particle. As a result, the initial fibrous structure morphology of the metallic nickel was gradually turned into pear-like shapes.

Keywords: Ni Catalyst; Ethylene glycol; Fibrous shape; Methane decomposition; Carbon nanofiber

1. Introduction

Catalytic decomposition of methane has recently received much attention as a potentially economical route for producing CO-free hydrogen that can be used directly as a fuel for H_2–O_2 cells [1–3]. Ni-based catalysts were extensively studied for methane decomposition due to their relatively higher activities compared with other transition metals [3–6]. Because the catalytic activity of the Ni catalysts decreased with time on stream due to the continuous deposition of carbons, the effective catalyst should exhibit sufficient carbon storage capacity on a per-gram basis of nickel, in addition to reasonable activity toward methane decomposition at relatively lower temperatures.

Because the most important factor influencing carbon yield during methane decomposition is the particle size of the metallic nickel, much attention has been given to disperse and stabilize nickel particles by selecting the appropriate support [7–12]. Metallic nickel supported on oxides has been the most commonly used catalysts for methane decomposition. It was reported that a typical 40%Ni/SiO_2 catalyst could give a carbon yield as high as 491 g_C/g_{Ni} during methane decomposition at 773 K [11]. Using niobium oxide (Nb_2O_5) to support 50.8%Ni and 21.2% of copper as a promoter, the yield of deposited carbon from methane reached 743 g_C/g_{Ni} at 873 K [12]. It was also found that 75%Ni–15%Cu–Al_2O_3 catalysts prepared by coprecipitation provided a carbon yield of 700 g_C/g_{Ni} at 898 K [10]. When taking into account the application of carbon fibers, however, the catalyst components should be removed or separated from the deposited carbons [13,14]. Nickel can be practically and easily removed by leaching with acidic aque-

* Corresponding author. Fax: +86 411 84694447.
E-mail address: shen98@dicp.ac.cn (W. Shen).

0021-9517/$ – see front matter
doi:10.1016/j.jcat.2005.12.027

ous, but the separation of the support materials, like Al_2O_3 and SiO_2, may be quite burdensome [15]. Thus, various carbons were used to support the nickel particles, and a secondary carbon yield of 268.5 g_C/g_{Ni} was obtained over a Ni/CFC (catalytic filamentous carbon) catalyst [16]. Obviously, the carbon-supported nickel catalyst usually gave a much lower carbon yield compared with that of the Ni particles supported by metal oxides [15,16].

To improve the overall efficiency of the process, attempts were made to prepare pure nickel catalysts without a textural promoter. Unfortunately, the pure Ni catalyst showed rapid deactivation due to the severe aggregation of nickel particles under reaction conditions and gave a much lower carbon yield ($\sim$10 g_C/g_{Ni}). But the addition of 10% Al_2O_3 or SiO_2 caused a nickel particle size decrease from 65 to 11 nm and carbon yields of 161–385 g_C/g_{Ni} [7,9]. Clearly, the textural promoter is the crucial component in formulating the effective nickel catalysts, and their role is to stabilize the easily aggregated metallic nickel particles. Perhaps for this reason, there still has been no successful report on using pure Ni catalyst for methane decomposition with reasonable activity and acceptable carbon storage capacity.

Meanwhile, it is also interesting to note that the synthesis of nickel oxides with controlled particle sizes and morphologies is becoming one of the hot topics in recent materials sciences. Thermal decomposition of solid nickel precursors, like nickel sol–gel complex and nickel hydroxides, were used to produce nanocrystalline NiO materials [17,18]. These prepared NiO materials are nearly spherical nanoparticles and thus tend to aggregate into rather larger particles when calcined at higher temperatures. The reported NiO materials gave small particle sizes ($<$10 nm) only after calcination at low temperature ($\leqslant$673 K), whereas the NiO particles rapidly aggregated into very large nanoparticles ($>$20 nm) after high-temperature calcination ($\geqslant$973 K). Meanwhile, there have been only few reports on the morphology-controlled synthesis of NiO materials. Nanorings and nanosheets of nickel oxides have been prepared by thermal calcinations of the corresponding β-$Ni(OH)_2$ [19,20]. But these studies were aimed at preparing nanosized NiO materials with specific morphological shapes, and little attention was paid to their catalytic applications.

In the present study, pure nickel oxides with controlled crystalline sizes and morphologies were successfully prepared by precipitation of nickel acetate and sodium carbonate aqueous solution with the mediation of ethylene glycol. The influence of preparation parameters on the physical properties of the nickel oxides and the catalytic behaviors for methane decomposition of the obtained Ni catalysts was extensively investigated by X-ray diffraction (XRD), temperature-programmed reduction (TPR), and transmission electron microscopy (TEM) techniques. The crystalline size and the morphological features of Ni were correlated with the catalytic activity of methane decomposition by following the evolution of nickel oxides to metallic nickel particles during hydrogen reduction and subsequent methane decomposition.

2. Experimental

2.1. Preparation of NiO catalysts

The nickel oxides were prepared by precipitation of nickel acetate dissolved in ethylene glycol with sodium carbonate aqueous solution at 353–433 K. A solution containing 0.05 mol of nickel acetate ($Ni(OAc)_2 \cdot 4H_2O$) and 150 mL of ethylene glycol (EG) was gradually heated to the desired temperatures (353–433 K) under stirring and maintained at the same temperature for 30 min. Then 500 mL of 0.2 M Na_2CO_3 aqueous solution was slowly added to the Ni-EG solution, with a final pH value of about 10. The precipitate was aged in the mother liquid for another 1 h. After being filtered and washed thoroughly with distilled water, the nickel hydroxide precipitate was dried at 373 K overnight and finally calcined in air at 673 K for 4 h. Depending on the precipitation temperature, the obtained solid was designed as NiO-EG-T, where T refers to the temperature of precipitation (in K).

For comparison, a NiO sample was also prepared by precipitation of nickel acetate dissolved in water with sodium carbonate aqueous solution at 353 K in the same procedure described above. The sample thus obtained was designed as NiO-H_2O-353.

To investigate the effect of calcination temperature on the physiochemical properties and catalytic features of the NiO materials, the nickel hydroxide precipitate prepared in the solution of ethylene glycol at 393 K was further calcined in air at 773–1073 K for 4 h, resulting in NO samples of varying crystalline sizes and morphologies.

2.2. Catalyst characterization

The N_2 adsorption–desorption isotherms were performed using a Nova 4200e (Quantachrome) system operated at 77 K. Before these measurements, the sample was degassed by vacuum at 573 K for 5 h. The BET surface area was calculated from a multipoint BET analysis of the nitrogen adsorption isotherms.

The X-ray powder diffraction (XRD) patterns were recorded on a D/MAX 2500 X-ray diffractometer (Rigaku), using Cu-K_α radiation operated at 40 kV and 100 mA. In situ XRD measurements for the reduction of the NiO samples were performed in a high-temperature chamber installed in the diffractometer. The NiO was pressed into flakes and mounted in the chamber. After heating to 773 K in the flow of Ar, pure hydrogen was introduced into the chamber and kept at 773 K for 1 h, after which the XRD patterns were recorded. The mean crystallite sizes of nickel and NiO were calculated from the Scherrer equation, where the particle shape factor was taken as 0.9 [21].

The TEM images were obtained with a JEOL JEM-2000EX operated at 100 kV. The HRTEM images were obtained with a Philips Tecnai $G^2$20 operated at 200 kV. Specimens were prepared by ultrasonically suspending the sample in ethanol. A drop of the suspension was then applied onto clean holy copper grids and dried in air. For TEM observation of the Ni catalyst, the NiO sample was first reduced with hydrogen in

a continuous-flow fixed-bed reactor at 773 K for 1 h. After being cooled to room temperature under Ar flow, anhydrous ethanol was introduced through a syringe pump with Ar as a carrier gas until the reduced sample was completely immersed. Then it was quickly transferred and stored in the bottle of ethanol.

Temperature-programmed reduction (TPR) was performed in a conventional setup equipped with a thermal conductivity detector. In typical runs, 50 mg NiO samples were used and heated to 673 K (10 K/min) under N_2 flow (40 mL/min) and kept at this temperature for 0.5 h to remove the adsorbed carbonates and hydrates. After cooling down to room temperature and introducing the reduction agent of 20 vol% H_2/N_2 (40 mL/min), the temperature was then programmed to rise from 303 to 1073 K at a ramp rate of 10 K/min.

Raman spectroscopes of the deposited carbon nanofibers were obtained over a homemade UV Raman spectrometer. A 325-nm laser line from Kimmon was chosen as the excitation source. The power of the UV laser line was 4.0 mW. The wavenumber of Raman spectra was corrected, and the spectra error was ± 2 cm^{-1}. The value of I_D/I_G was estimated by curve-fitting of the Raman spectrum using Gauss function.

2.3. Catalytic activity test

Methane decomposition reaction was carried out in a continuous-flow fixed-bed quartz reactor at 773 K under atmospheric pressure. A 40-mg sample of NiO (40–60 mesh) was loaded and prereduced with pure hydrogen (20 mL/min) at 773 K for 1 h before the reaction. The Ni catalyst was then flushed with Ar for 0.5 h. CH_4 (99.995% purity, 60 mL/min) was then introduced with a gas hourly space velocity of 90,000 mL/(g_{cat} h) through a mass flow controller. To eliminate the space limitation for carbon growth, the reactor had an internal diameter of 28 mm and length of 250 mm. The effluents from the reactor were analyzed by on-line gas chromatography. Over all of the catalysts, hydrogen was detected as the only gaseous product, indicating that methane decomposition occurs selectively as $CH_4 \rightarrow 2H_2 + C$. Accordingly, methane conversion was calculated from the amounts of hydrogen produced.

3. Results and discussion

3.1. Effect of preparation parameters

Fig. 1 shows the XRD patterns of the nickel oxides obtained by calcination of the nickel hydroxide precipitates at 673 K, which were prepared in water and ethylene glycol. Clearly, all of the samples showed a typical face-center cubic structure of NiO (JCPDS#4-835). The NiO-H_2O-353 had the largest crystalline size (8.4 nm) and a surface area of 78 m^2/g. The crystalline sizes and the surface areas of the samples prepared in ethylene glycol were strongly dependent on the precipitation temperature. Precipitation at 353 and 433 K resulted in similar NiO crystalline sizes of 6.8–7.1 nm and close surface areas of 78–93 m^2/g, whereas the NiO-EG-393 sample gave

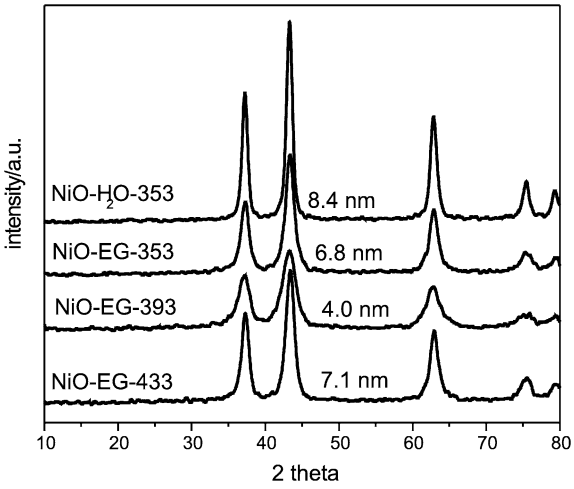

Fig. 1. XRD profiles of the nickel oxides.

the smallest crystalline size (4.0 nm) and the largest surface area (123 m^2/g). Fig. 2 gives the corresponding TEM images of the nickel oxides. Clearly, the morphology was determined by the preparation conditions as well. Precipitation in water led mainly to the formation of spherical particles (10–20 nm) and a few nanorods of NiO. The morphology of the nickel oxides prepared in ethylene glycol solutions was significantly related to the precipitation temperature. The NiO-EG-353 sample exhibited aggregated spherical particles, and the NiO-EG-393 sample showed fibrous shapes and interlayered structures with no spherical particles. The NiO-EG-433 sample consisted of nanorods (mainly NiO) and spherical particles.

Fig. 3 illustrates the H_2-TPR profiles of the nickel oxides. The figure shows only one hydrogen consumption peak at 500–800 K, representing the characteristic reduction of stoichiometric nickel oxide [22]. Although the NiO-H_2O-353, NiO-EG-353, and NiO-EG-433 samples have different crystalline sizes and particle shapes, they exhibited similar reduction features with a strong and sharp hydrogen consumption peak at around 600 K. This may indicate that there is little effect of crystalline size (6–8 nm) and morphology on the reduction behaviors of these nickel oxides. However, the NiO-EG-393 sample exhibited a relatively broad hydrogen consumption peak at higher temperature (700 K), suggesting that reduction of the NiO species is relatively difficult. It was previously stated that the reduction temperature of NiO increased with increasing crystalline size in the range of 6–17 nm [18], but there have been only a few reports on the effect of morphology on the reduction property of NiO. For the current NiO-EG-393, the calculated crystalline size of NiO was only 4.0 nm, and it should be practically and easily reduced into metallic Ni at lower temperatures. But its reduction was completed at a higher temperature than the other samples with larger NiO crystallines. Therefore, it is reasonable to speculate that the interlayered structure of the NiO-EG-393 sample hindered the reduction of NiO. In fact, H_2-TPD studies of a Ni/SiO_2 catalyst have already revealed that the morphology can indeed influence the desorption characteristics of metallic nickel, and the nickel in whisker shapes is more reactive toward hydrogen than spherical nickel [23,24]. Accord-

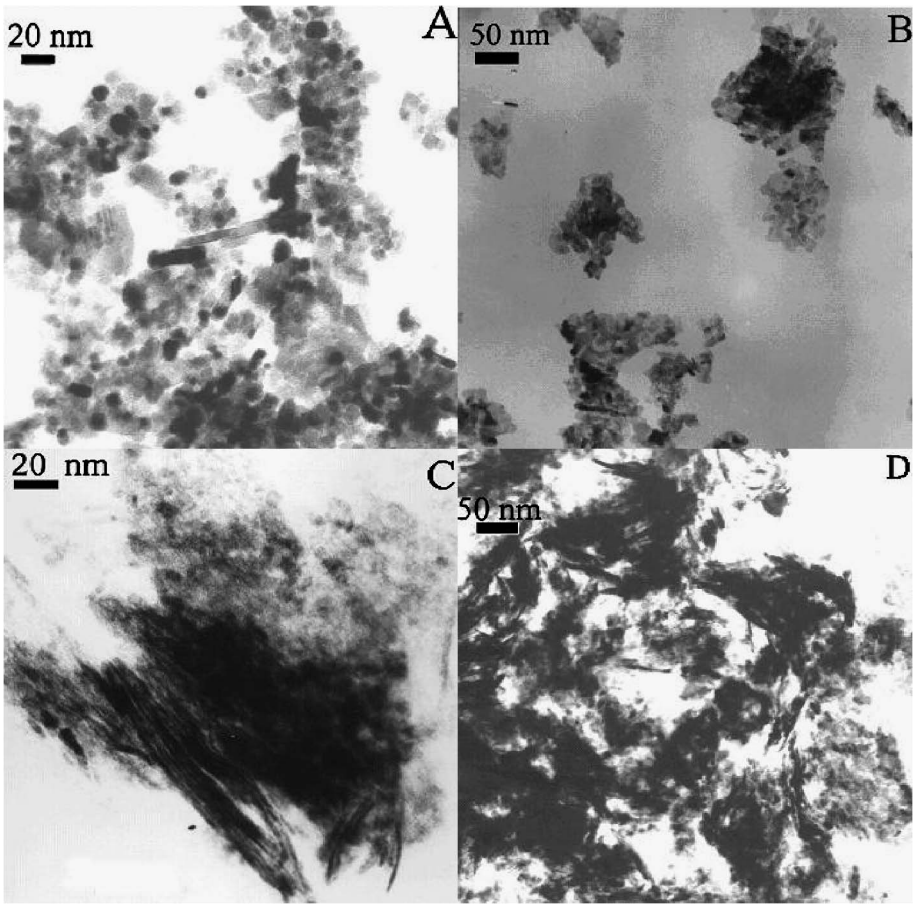

Fig. 2. TEM images of the nickel oxides: (A) NiO-H_2O-353, (B) NiO-EG-353, (C) NiO-EG-393, (D) NiO-EG-433.

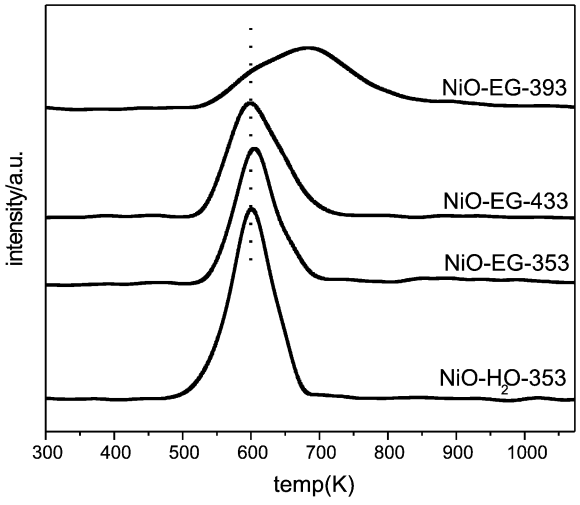

Fig. 3. TPR profiles of the nickel oxides.

ingly, the interlayered structure of fibrous NiO may be rather stable under hydrogen atmosphere compared with the spherical particles and thus may lead to significant differences in the reduction features compared with other samples with spherical NiO particles.

3.2. Methane decomposition

The NiO samples were first reduced into metallic nickel with hydrogen at 773 K, and then tested for methane decomposition. Fig. 4 depicts the methane conversions as a function of time-on-stream, and the accumulated carbon decomposition and hydrogen yield were accordingly calculated. It is surprising that the NiO-H_2O-353 did not show any catalytic activity toward methane decomposition, whereas the NiO samples prepared in the solution of ethylene glycol showed differing catalytic activities, depending on the precipitation temperature. The NiO-EG-353 sample exhibited pronounced catalytic activity for methane decomposition with 60 h of time on stream, with accumulated carbon and hydrogen yields of 271 g_C/g_{Ni} and 2651 mol_{H_2}/mol_{Ni}, respectively. The NiO-EG-393 sample gave the highest methane conversion with rather prolonged catalytic activity for 75 h, and the accumulated carbon and hydrogen yields approached 398 g_C/g_{Ni} and 3894 mol_{H_2}/mol_{Ni}. However, the NiO-EG-433 sample gave only marginal methane conversions for about 5 h, and the accumulated carbon and hydrogen yields were calculated as 3.4 g_C/g_{Ni} and 33 mol_{H_2}/mol_{Ni}. Thus, it seems true that both the precipitation media and the precipitation temperature play crucial roles in determining the catalytic properties of the Ni catalysts, probably through effective control of the crystalline and/or particle size as well as the morphology of the nickel hydroxide precipitates and the nickel oxides. In particular, precipitation in ethylene glycol at 393 K led to the formation of stable α-$Ni(OH)_2$ with hydrotalcite-like structure, and further calcination of this nickel hydroxide resulted in the formation of NiO-EG-393 with fi-

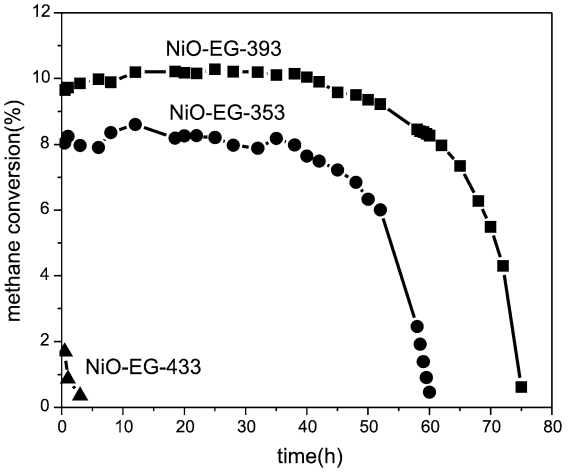

Fig. 4. Methane conversion as a function of time-on-stream over the Ni catalysts originated by hydrogen reduction of the nickel oxides at 773 K. (Reaction temperature, 773 K; catalyst, 0.040 g; methane, 101 kPa; and flow rate, 60 mL/min.)

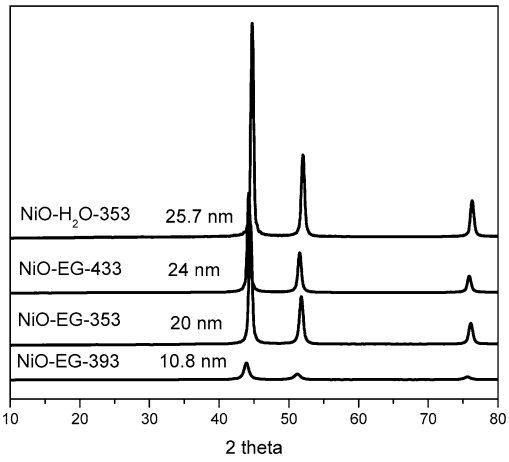

Fig. 5. XRD patterns of the Ni catalysts obtained by hydrogen reduction of the NiO precursors at 773 K.

brous shapes. Unsupported Ni catalysts have been prepared by conventional precipitation method in aqueous solution and also tested for methane decomposition in previous studies [7,9]. But these pure Ni catalysts only gave very low carbon yields of about 10 g_C/g_{Ni}, similar to case of the NiO-EG-433. When small amounts of Al_2O_3 or SiO_2 were used to support the nickel oxides, considerable increases in carbon yields (161–384 g_C/g_{Ni}) were observed. Notably, the carbon yield of 398 g_C/g_{Ni} achieved over the NiO-EG-393 was slightly higher than the most promising value of 384 g_C/g_{Ni} over a 90%Ni/SiO_2 catalyst reported to date [9]. Thus, the Ni catalyst prepared by precipitation of nickel acetate at 393 K with the mediation of ethylene glycol could be an excellent candidate for methane decomposition.

3.3. Particle size and morphology of the reduced metallic nickel

From the reaction results of methane decomposition, it seems that the initial particle size and morphology of nickel oxide precursors had important effects on the catalytic performance of the reduced Ni catalysts. Because the metallic nickel generated from hydrogen reduction of NiO is the active component for methane decomposition, it is necessary to establish the relationship between the particle or crystalline size of the metallic nickel and the methane conversion. Fig. 5 shows the XRD patterns of the Ni catalysts obtained by reduction of NiO samples with hydrogen at 773 K. It can be seen that NiO was completely reduced to metallic nickel (JCPDS#4-850). Clearly, the crystalline sizes of metallic nickel were greatly increased (by about threefold) compared with their corresponding NiO precursors (Fig. 1). If the nickel crystalline size is correlated to the catalytic behavior of methane decomposition, then it can be readily seen that the metallic Ni with crystalline size of about 10.8 nm had the highest carbon and hydrogen yields and that the metallic Ni with crystalline size of about 20 nm produced a relatively lower carbon yield. Increasing the Ni crystalline size to about 24 nm led to extremely low catalytic activity, and further increasing the size up to 26 nm resulted in total inactivity toward methane decomposition. Thus, it appears that the metallic nickel with crystalline size of 10–20 nm is suitable for methane decomposition. The methane decomposition reaction depends critically on the crystalline size of metallic nickel, with dramatically decreased catalytic activity with increasing crystalline size. This observation is consistent with previous reports concerning the effect of Ni crystalline size on methane decomposition over various supported nickel catalysts. Investigation of methane decomposition over a series of 90%Ni/SiO_2 catalysts revealed that nickel crystalline sizes of 10–40 nm gave similar carbon yields of 300–384 g_C/g_{Ni}, whereas further increasing the nickel crystalline size to 60 nm drastically decreased the carbon yield to 2 g_C/g_{Ni} [9]. Similarly, 96%Ni/SiO_2 catalysts with nickel crystalline sizes of 20 nm showed the highest carbon yield of 300 g_C/g_{Ni}, and the carbon yields greatly decreased (to 222 and 107 g_C/g_{Ni}) when Ni crystalline sizes were slightly increased (to 25 and 38 nm, respectively). For lower nickel loading systems, studies over a 15%Ni/CFC catalyst also concluded that Ni crystalline sizes of 30–70 nm were suitable for the growth of carbon filaments during methane decomposition [8,25]. The most effective crystalline size of Ni for the growth of filamentous carbon was found to be 10–60 nm over a 23.3%Ni/SiO_2 catalyst [26]. It was further observed that the optimal growth rate of carbon nanofibers could be achieved over Ni crystals around 34 nm in size if supported by hydrotalcite materials [27].

Although it is obvious that smaller Ni crystalline sizes show higher catalytic activity for methane decomposition, there is a significant discrepancy among the reported optimal metallic nickel crystalline sizes for methane decomposition, which strongly depends on the support and the Ni loading. For the current unsupported Ni catalysts, metallic nickel with crystalline size of 10–20 nm was found to be suitable for methane decomposition, but increasing the crystalline size to 26 nm resulted in total inactivity. This extreme sensitivity of metallic nickel

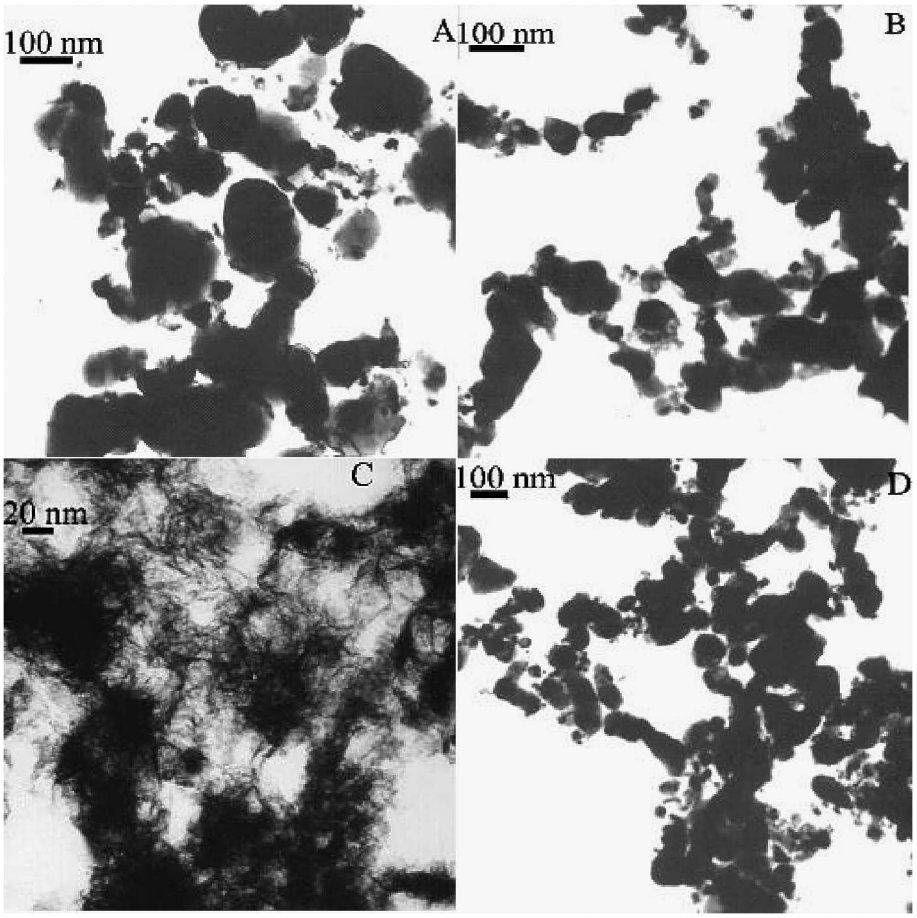

Fig. 6. TEM images of the Ni catalysts obtained by hydrogen reduction of (A) NiO-H_2O-353, (B) NiO-EG-353, (C) NiO-EG-393, and (D) NiO-EG-433 at 773 K.

crystalline size up to 26 nm implies that other factors may be governing the reaction of methane decomposition, such as the morphology of the reduced Ni and the structural evolution under reaction conditions.

Fig. 6 provides TEM images of the reduced Ni catalysts. It can be seen that the NiO samples with some spherical particles changed to regular spherical shapes after reduction with hydrogen at 773 K. The NiO-H_2O-353 with spherical NiO particles (10–20 nm) and few nanorods exhibited 100–200 nm metallic Ni particles. The NiO-EG-353 with aggregated spherical NiO particles showed a change to large Ni particles (30–100 nm). The NiO-EG-433 containing nanorods and spherical particles of NiO were all reduced to spherical Ni particles (50–100 nm). This may suggest that the NiO species with nonspherical shapes in these samples were not stable under hydrogen reduction conditions and finally aggregated into large Ni spherical particles. However, it is quite interesting to note that even though hydrogen reduction at 773 K of the fibrous shape of the NiO-EG-393 sample resulted in the formation of fibrous metallic Ni, no spherical particles were observed. The finding of rather stable fibrous shapes in the NiO-EG-393 sample is very promising for NiO and metallic nickel nanomaterials, because the previously reported nickel oxide and metallic nickel over supporting materials for methane decomposition were all of spherical shape [9,17]. Boudjahem et al. successfully prepared silica-supported whisker-like metallic nickel by reduction of nickel acetate with hydrazine and showed that this new morphology of metallic nickel was more active for benzene hydrogenation and more selective in acetylene hydrogenation to benzene [23,24]. However, this nonclassical nickel phase can be obtained only for very low nickel loading (<2%), and the silica support must be of very low surface area (15 m^2/g). To date, there have been no reports on preparing pure NiO and metallic Ni with the fibrous structures as observed in the NiO-EG-393 sample, and the metallic nickel with such a unique morphology exhibited much higher catalytic activity for methane decomposition than the conventional spherical metallic nickel.

3.4. Evolution of nickel particles during CH_4 decomposition

It was recently proposed that the nickel catalysts might be considered as self-organizing systems during the reaction of methane decomposition [15,28]. Nickel particles underwent active evolution and gradually stabilized at thermodynamically favorable sizes. Therefore, the NiO samples were reduced into metallic Ni catalysts with hydrogen at 773 K and reacted with methane for desired periods. XRD measurements and TEM observations were then conducted to follow the evolution of the nickel particles. Fig. 7 shows the XRD patterns of the freshly reduced Ni and the completely deactivated samples. Because the typical diffraction peak of Ni (111) was overlapped with the graphite (101) plane, the crystalline sizes were calculated ac-

cording to the half-width of the diffraction peak of the Ni (200) plane. It can be seen that the crystalline size of nickel increased noticeably during the first 30 min, and no further pronounced increase was observed in the following reaction course. The nickel crystalline size increased slightly (from 20 to 23 nm) over the NiO-EG-353 sample, whereas the nickel crystalline size increased significantly (from 10.8 to 17–18 nm) over the most effective NiO-EG-393 sample. The change in metallic nickel crystalline size at the initial stage of methane decomposition implied that the deposited carbon would induce aggregation of the fine Ni crystallines into larger sizes. But the nickel crystalline size increased only marginally (from 24 to 26 nm) in the NiO-EG-433 sample, which showed the lowest catalytic activity. This critical Ni crystalline size of 26 nm is in good agreement with the findings for the NiO-H_2O-353 sample in which the reduced metallic nickel crystalline size was 26 nm and showed no activity for methane decomposition. Thus, it can be speculated that nickel crystals larger than 26 nm are not active for methane decomposition. This can be understood by considering the dissociation of methane on Ni crystals. Generally, methane is adsorbed and decomposed on a certain face of Ni, followed by the diffusion and deposition of carbon atoms on the surface of nickel crystals. The catalytic life is determined by the ratio of the formation rate of carbon atoms on the Ni metal surfaces to the diffusion rate approaching the deposit site. Thus, there should be an optimal size of active Ni crystals that could achieve this dynamic equilibrium for longer periods [7,9,11]. Avdeeva et al. studied the evolution of nickel particles over a 75%Ni/Al_2O_3 catalyst during methane decomposition and found that the nickel crystalline size increased from the initial 9 to 16.5, 22.5, and 40 nm after reaction with methane for 20, 60, and 180 min, respectively [7]. Accordingly, these authors concluded that the formation of large Ni crystals during the reaction is likely caused by the dissolution of the carbon into the metal. Based on the XRD measurements of a series of 90%Ni/SiO_2 catalysts, Ermakova et al. stated that the nickel crystalline sizes merged from 15 to 30 nm or dispersed from 60 to 30 nm during the reaction of methane decomposition and that the active nickel crystalline sizes stabilized at 30–40 nm [28]. Reshetenko et al. reported that the Ni crystalline size increases from the initial 13 to 27 nm over a 75%Ni-15Cu%-Al_2O_3 catalyst after reaction with methane for 10–20 min at 898 K [10]. Studies on the relationship between nickel crystalline size and the catalytic activity of methane decomposition have suggested that the deposited carbons over Ni catalysts supported by carbon fibers modified the size of the Ni crystallites during the reaction, and that nickel crystallites about 20 nm in size were the most active sites for the growth of carbon nanofibers [15]. From this standpoint, the observed optimal Ni crystalline size of 17–23 nm for the current NiO catalysts is in good accordance with previous conclusions concerning Ni crystalline evolution under methane decomposition conditions.

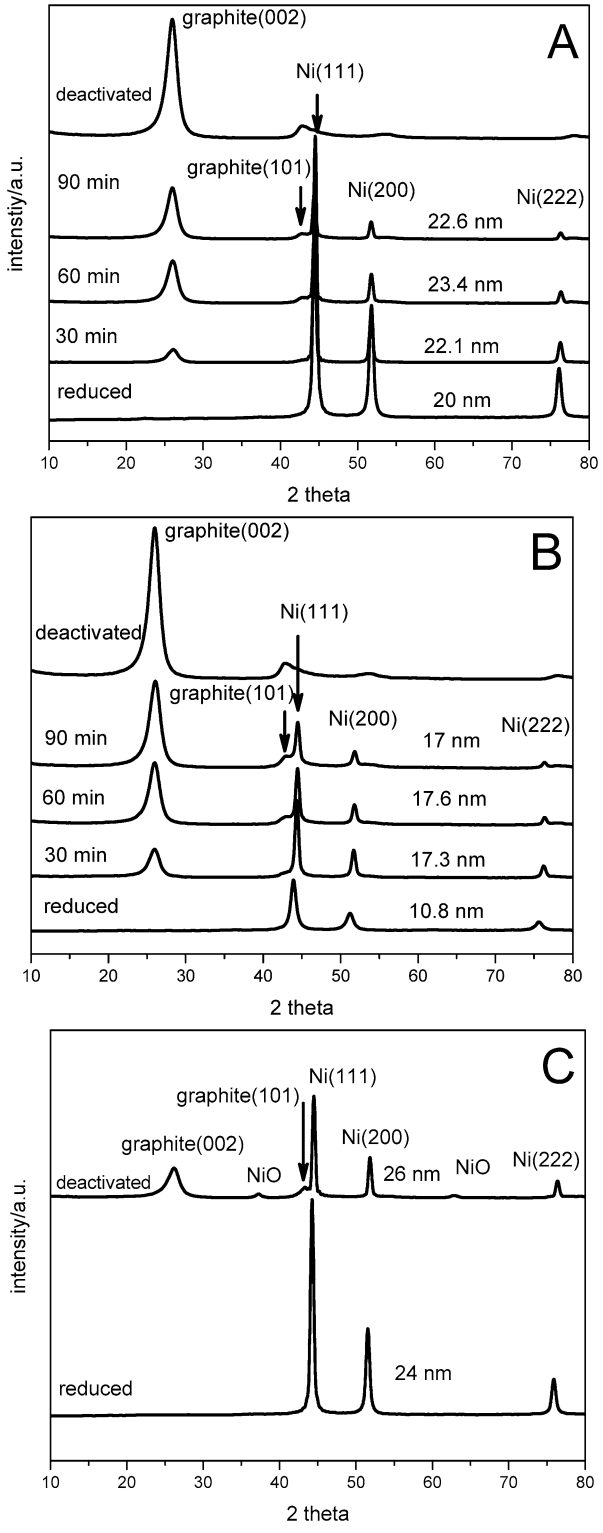

Fig. 7. XRD profiles of the Ni catalysts after exposure to methane decomposition: (A) NiO-EG-353, (B) NiO-EG-393, (C) NiO-EG-433.

Fig. 8 further compares the TEM images of the deposited carbons on the Ni catalysts after complete deactivation during methane decomposition. Significant difference in the morphologies of the deposited carbon can be clearly seen. For the NiO-EG-353 and NiO-EG-393 samples, which were active for methane decomposition, the carbons were all in nanofiber form. The nickel particles (darker spots) were all located at the tips of carbon nanofibers, and the diameters of the Ni particles were almost the same as those of the growing nanofibers. The NiO-EG-433 K sample, which was rapidly deactivated within 5 h

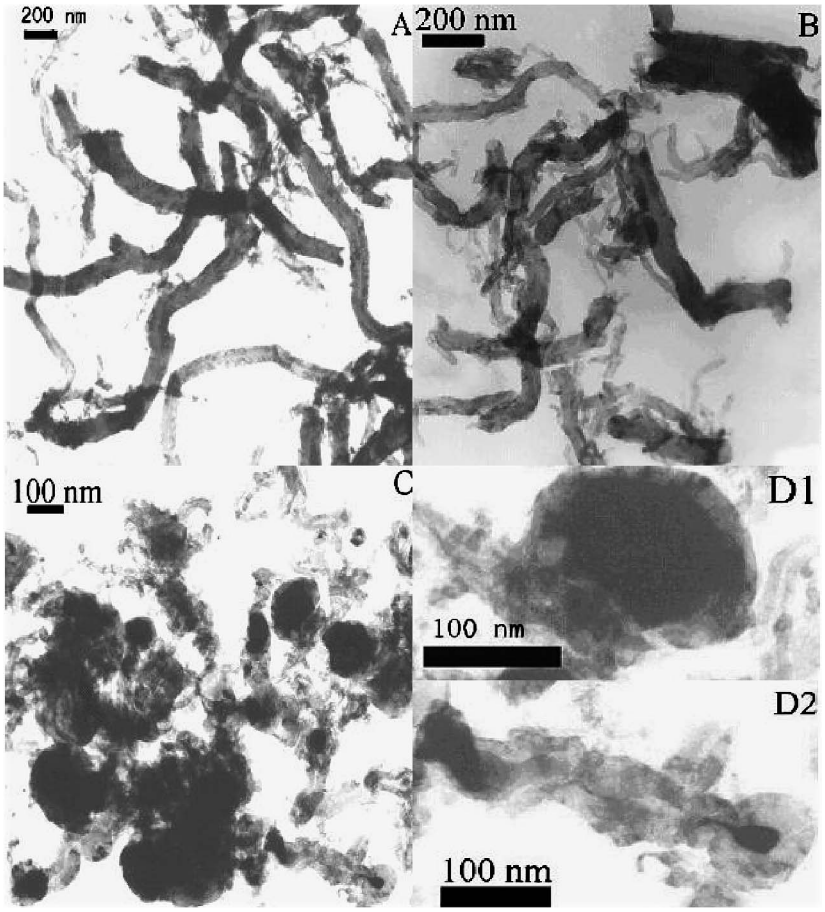

Fig. 8. TEM images of the completely deactivated Ni catalysts: (A) NiO-EG-353, (B) NiO-EG-393, (C) NiO-EG-433, (D1)–(D2) enlargement part of NiO-EG-433.

time on stream, exhibited three types of Ni particles after complete deactivation. The smaller Ni particles (ca. 30 nm) with elongated shapes tended to form carbon nanofibers, the relatively large Ni particles (ca. 100 nm) were encapsulated by graphitic carbon that greatly inhibited the contact of Ni particles with methane, and the largest Ni particles (>100 nm) produced no carbon around them. These findings confirm that the particle size of metallic nickel also plays an important role in the process of methane decomposition. It also provides convincing evidence that Ni particles >100 nm cannot perform methane decomposition, thus explaining the total inactivity of the NiO-H_2O-353 catalyst (because the Ni particles after hydrogen reduction were already >100 nm). This TEM observation is also similar to the previous results. Takenaka et al. reported that 60–100 nm Ni particles estimated from SEM images exhibited the longest catalytic life for methane decomposition over a 40%Ni/SiO_2 catalyst [11]. Shaikhutdinov et al. demonstrated, using TEM, that 30–70 nm Ni particles were more active for the growth of carbon filaments than other particles [8].

3.5. Optimal Ni particle size

There are significant discrepancies among the reported nickel crystalline and/or particle sizes suitable for methane decomposition, usually based on XRD and TEM observations. The particle sizes measured by TEM or SEM observations and the crystalline sizes obtained from XRD profiles should be clearly distinguished. The former usually gives individual particle sizes that are the aggregation of various Ni crystals, whereas the latter can give only the average crystalline size of nickel. Comparing the two approaches in terms of Ni crystalline size, previous reports have focused on supported Ni catalysts in which the Ni particles were all of spherical shape and the proposed optimal Ni crystalline sizes obtained from XRD measurements were mainly in the range of 20–40 nm. In the present work, pure Ni crystalline of particle size <23 nm showed quite pronounced catalytic activity for methane decomposition, and a slight increase in the nickel crystalline size to 26 nm resulted in total deactivation for methane decomposition. This relatively narrower Ni crystalline size range may be due to the lack of support. Besides stabilizing the Ni particles, the support may also provide deposition sites for the growth of the carbon diffused from Ni [29,30]. The absence of support in the pure Ni catalysts requires that the nickel crystalline have high activity toward methane cracking and also sufficient ability to facilitate the immediate growth of carbon filaments. Such a balance between the formation rate of carbon atoms on the Ni surfaces and the diffusion rate approaching the deposit site make the reaction more sensitive over unsupported Ni catalysts.

Considering the particle sizes observed by TEM images, spherical Ni particles >100 nm could not produce any carbon;

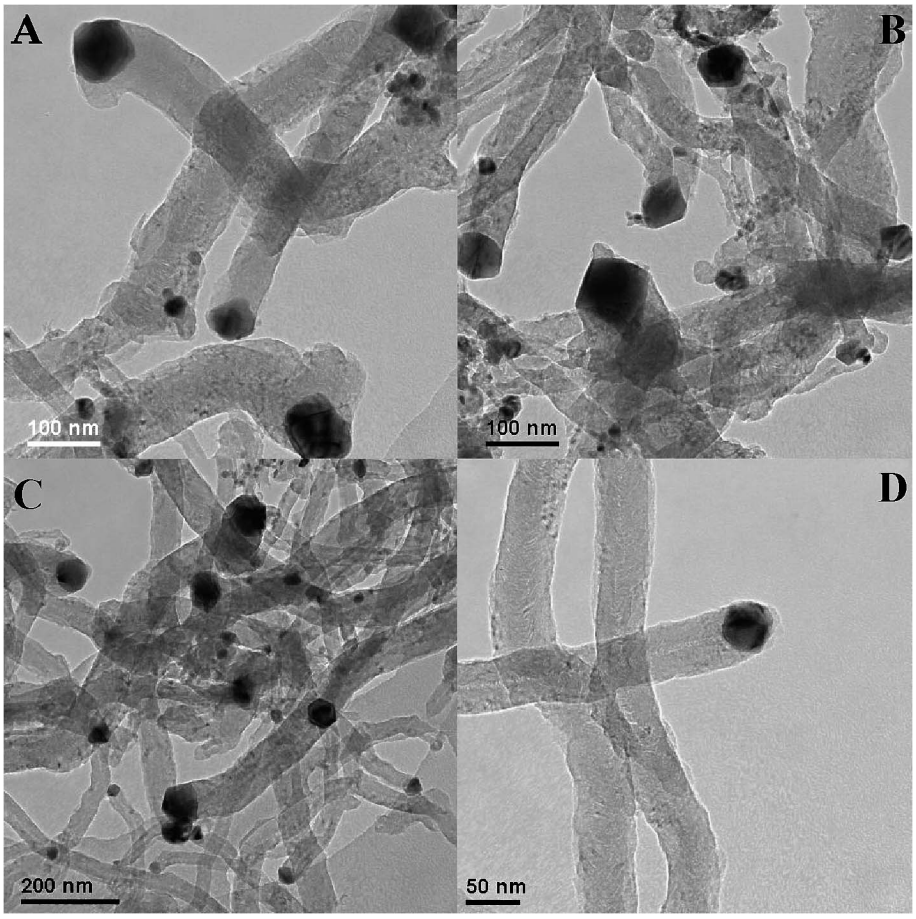

Fig. 9. HRTEM images of the carbon nanofibers formed by methane decomposition over the Ni catalyst obtained by hydrogen reduction of NiO-EG-393 at 773 K: (A) 30 min, (B) 60 min, (C) 90 min, and (D) carbon nanofiber.

only the small Ni particles produced significant amounts of carbon nanofibers. As a result, the Ni-H_2O-353 and Ni-EG-433 samples containing mainly Ni particles >100 nm did not show promising catalytic activities. When the reduced Ni is presented as nonspherical shapes, the comparison in terms of particle size becomes controversial. In the fibrous NiO-EG-393 sample, fibrous Ni was observed with a crystalline size of 10.8 nm, and this highly active nickel further grew into larger crystals of 17–18 nm during the reaction. The formation of Ni particles during the reaction should be related to this fibrous structure. As shown in Fig. 9, the deposited carbon grew with a filamentous structure. The nickel particles (darker spots) were all located at the tips of carbon nanofibers, and the diameters of the Ni particles were almost the same as those of the growing nanofibers. Initially, the 17–18 nm Ni crystalline effectively ignited the decomposition of methane and induced the growth of carbon nanofibers around it. As the reaction proceeded, the Ni crystallines departed from the fibrous structures and gradually aggregated into particles over the deposited carbons, which can be considered the in situ produced support. The nickel particles were then highly dispersed on the carbon nanofibers, and simultaneously the initial fibrous structure morphology gradually changed to pear-like shapes. Thus, it can be concluded that the deposited carbon changed not only the sizes, but also the shapes of the nickel particles during methane decomposition. Together with the evolution of Ni particles, the structure of the deposited carbon nanofibers also changed with time on stream.

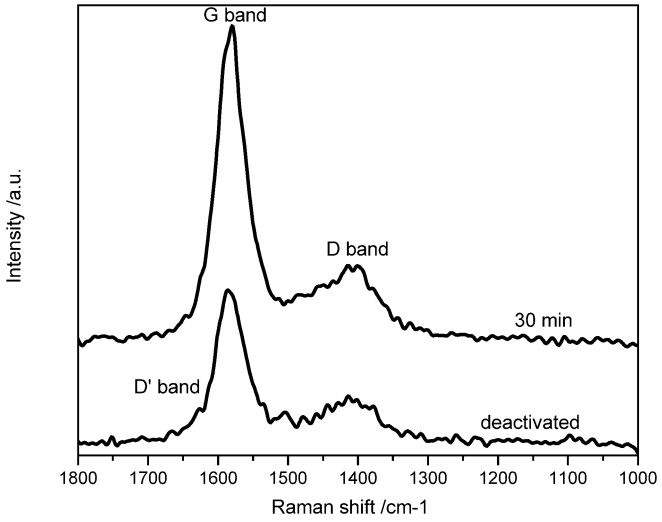

Fig. 10. Raman spectra of the carbons deposited by the methane deposition over the Ni catalyst originated from NiO-EG-393.

Fig. 10 shows the Raman spectra of carbons during methane decomposition over the Ni catalyst obtained by hydrogen reduction of the NiO-EG-393 sample. Two distinct bands

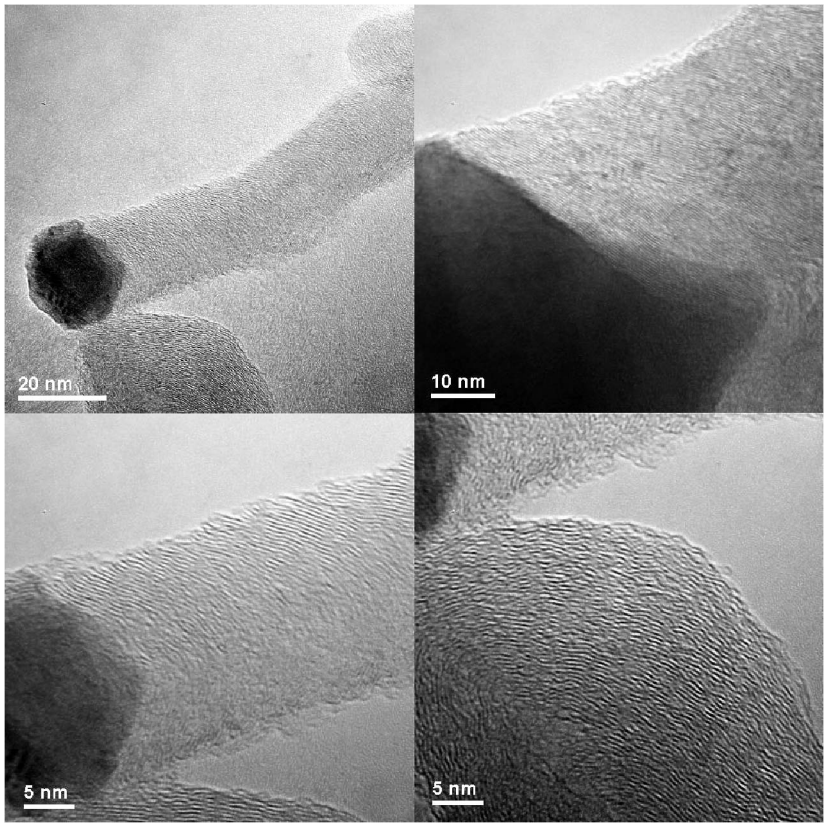

Fig. 11. HRTEM images of the deposited carbon over the Ni catalyst originated from NiO-EG-393. The sample was taken after 30 min reaction of methane decomposition.

were detected at about 1400 cm^{-1} (D band) and 1580 cm^{-1} (G band). The former is usually ascribed to the structural imperfection of graphite, and the latter is attributed to the in-plane carbon–carbon stretching vibrations of the graphite layers [11,31,32]. The shoulder peak at 1620 cm^{-1} (D′ band) was assigned to the imperfect graphite or disordered carbons [33,34]. The ratio of the area of the D band to that of the G band (I_D/I_G) was considered an index for the crystalline order of graphite [11,34–37]; that is, the graphitization degree of carbons is higher at lower I_D/I_G values. The I_D/I_G value calculated by curve-fitting of the Raman spectra in Fig. 10 increased from 0.44 to 0.82, indicating that the crystalline order of the deposited carbon was decreasing with the continuous growth of carbon nanofibers. Fig. 11 shows high-resolution TEM (HRTEM) images of deposited carbon nanofibers on the nickel catalysts at the early stage of methane decomposition. Obviously, the deposited carbon was pure nanofibers, and no other forms of carbon could be observed. The graphene layers were canted with respect to the longitudinal axis of the fibers, and Ni metal particles of pear-like shape presented at the tips of the carbon nanofibers.

3.6. Effect of calcination temperature on the NiO structure

Because the NiO-EG-393 sample with fibrous shape and rather small crystalline size exhibited excellent catalytic activity for methane decomposition, calcination of the nickel hydroxyl precursor was performed at 773–1073 K to reveal the interesting structural and catalytic features of the Ni catalysts. The crystalline size of NiO after calcination at 773 K was calculated as about 4.5 nm, and it increased only slightly to 8.1 nm even after calcination at 1073 K. Fig. 12 shows the corresponding HRTEM images of the NiO samples. It can be seen that the interlayer structure with fibrous shapes of NiO remained in all of the samples, even though the bundles were becoming shorter with increasing calcination temperature. Fig. 13 demonstrates the effect of calcination temperature on the catalytic activities of the Ni catalysts for methane decomposition. Interestingly, no significant changes in the methane conversions over these Ni catalysts were observed, even though the crystalline sizes of their NiO precursors were found to increase with calcination temperature. When the crystalline size of NiO increased from 4.5 to 8.1 nm, the carbon yield varied only slightly (between 381 g_C/g_{Ni} and 394 g_C/g_{Ni}), and the corresponding hydrogen yield also varied only slightly (between 3727 mol_{H_2}/mol_{Ni} and 3854 mol_{H_2}/mol_{Ni}).

The NiO samples obtained by calcining the nickel hydroxide precursor at 673 and 1073 K were selected to investigate the evolution of NiO and metallic Ni particles during the hydrogen reduction and the subsequent reaction of methane decomposition. Fig. 14 shows the XRD patterns measured during the reduction of nickel oxides with hydrogen. Clearly, the two catalysts showed similar reduction behaviors with increasing reduction temperature. The metallic nickel phase appeared after reduction at 573 K, and the diffractions of NiO almost vanished at 673 K. With further increases in reduction temperature,

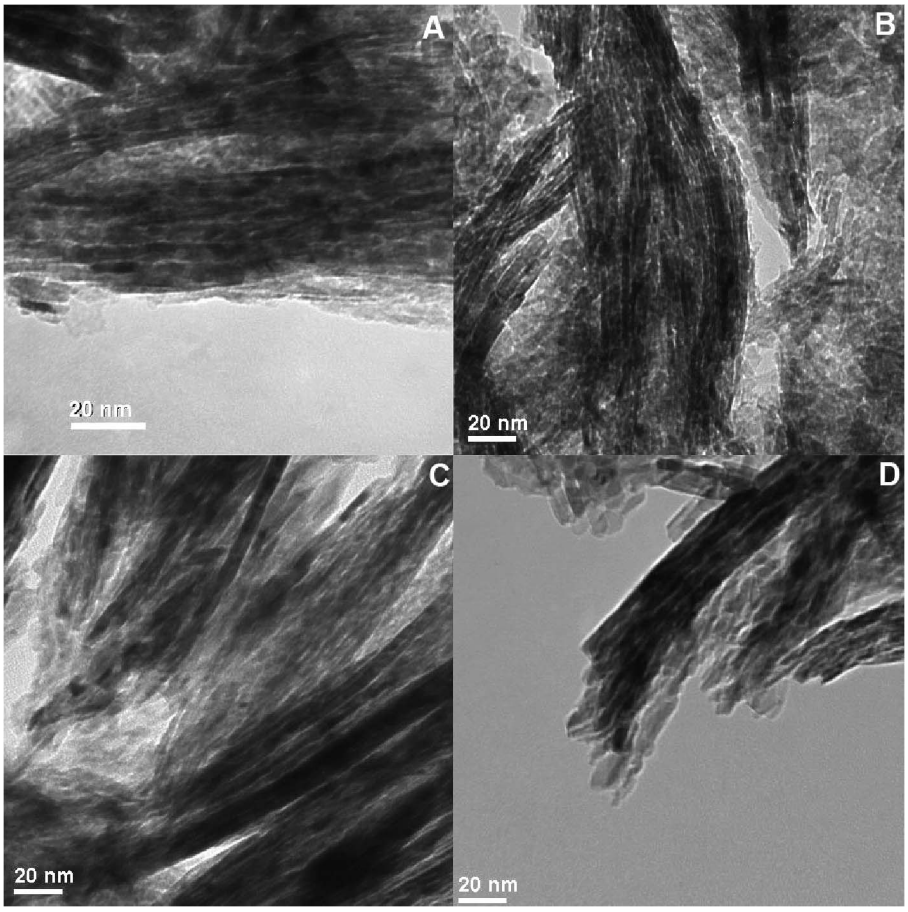

Fig. 12. HRTEM images of the NiO samples obtained by calcining the nickel hydroxide precipitate at 673–1073 K: (A) 673 K, (B) 773 K, (C) 973 K, (D) 1073 K.

the diffractions of metallic Ni gradually became extensive and sharper, indicating the enlarging metallic Ni crystallines. Although the initial crystalline sizes of the NiO samples were 4.0 and 8.1 nm, the resulting metallic Ni crystalline sizes were almost the same (about 9–11 nm) after reduction with hydrogen at 773 K. Fig. 15 shows the XRD profiles of the Ni crystalline during methane decomposition over the Ni catalyst generated from NiO by calcination of the precipitate at 1073 K. Similar to the case of the Ni crystalline size over the NiO-EG-393 sample (Fig. 7B), the fresh Ni metallic crystalline sizes in both catalysts were estimated to be ca. 10 nm, increasing significantly (to 17 nm) during the first 30 min under methane decomposition. Thereafter, no further changes could be observed, and the metallic Ni crystallines were stabilized at 17–18 nm. Clearly, the Ni catalysts prepared in the ethylene glycol solution at 393 K had different crystalline sizes after calcination at 673–1073 K, but similar metallic Ni crystalline sizes were obtained after reduction at 773 K with hydrogen. When further exposed to the reaction media, the metallic Ni crystallines still exhibited similar evolution behavior and rapidly stabilized at the critical size of 17–18 nm within 30 min. This phenomenon can explain the similar catalytic activities observed for methane decomposition over the NiO catalysts prepared in the solution of ethylene glycol at 393 K and calcined between 673 and 1073 K.

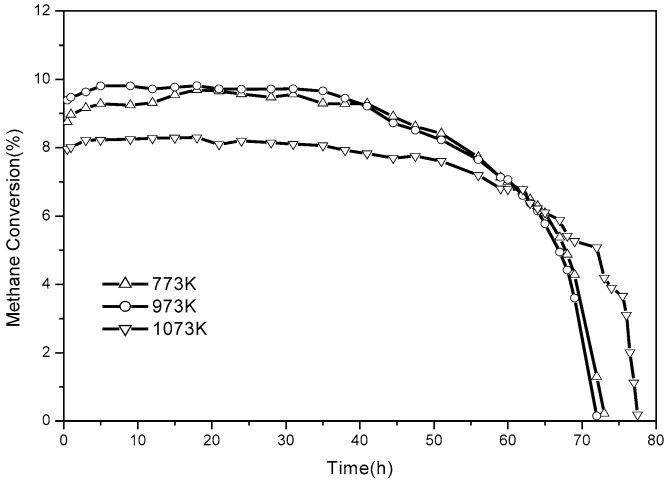

Fig. 13. Methane conversion as a function of time-on-stream over the Ni catalysts. NiO precursors were prepared by calcining the nickel hydroxide precipitate at 773–1073 K. (Reaction temperature, 773 K; NiO, 0.040 g; methane, 101 kPa; flow rate, 60 mL/min.)

4. Conclusion

Nickel oxides with controlled crystalline sizes and fibrous shapes were successfully prepared by the precipitation of nickel acetate and sodium carbonate aqueous solution with the me-

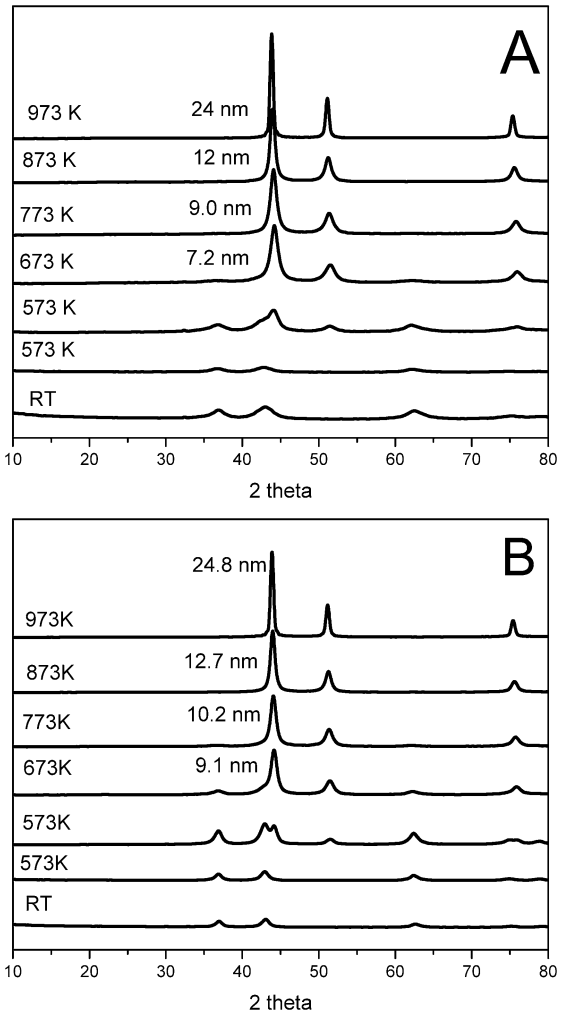

Fig. 14. XRD patterns of the nickel oxides during hydrogen reduction process. NiO was obtained by calcination of the nickel hydroxide at: (A) 673 K and (B) 1073 K.

diation of ethylene glycol. The precipitation temperature was found to play crucial role in determining the crystalline size and shape of the NiO samples. Precipitation at 393 K resulted in the formation of α-$Ni(OH)_2$ with a hydrotalcite-like structure, and further calcination of this precipitate precursor at 673–1073 K led to the formation of nickel oxides with layered structures. The crystalline size of the NiO after calcination at 673 K was 4.0 nm and increased only slightly to 8.1 nm even after calcination at 1073 K. On reduction with hydrogen at 773 K, the crystalline sizes of the obtained Ni catalysts were almost the same (9.0–11.0 nm). More importantly, the reduced nickel maintained the fibrous shapes of the initial NiO precursors.

The catalytic activity of the pure Ni catalysts for methane decomposition was strongly related to the crystalline size of the reduced Ni. The Ni catalyst with crystalline size of about 10.8 nm had the highest carbon and hydrogen yields, and the nickel crystalline of about 20 nm gave relatively lower carbon yields. Further increasing the nickel crystalline size to about 24 nm led to extremely low catalytic activity, and an increase up to 26 nm resulted in total deactivation toward methane decomposition. Further evolution of the Ni particles during methane

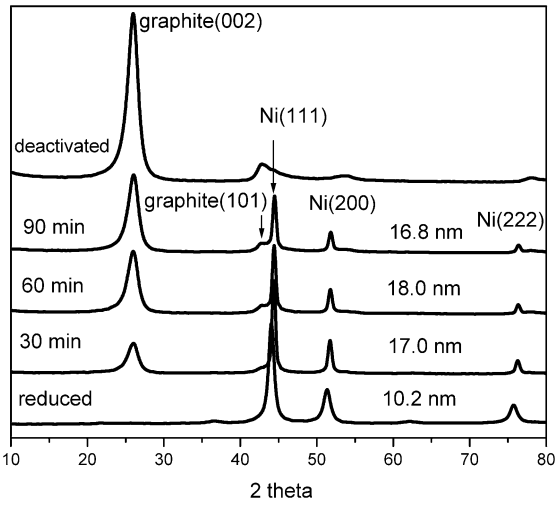

Fig. 15. XRD patterns of the NiO catalysts obtained by calcining the nickel hydroxide precipitate at 1073 K after exposure to methane decomposition.

decomposition reaction suggested that the deposited carbon changed not only the crystalline size, but also the morphology of the metallic nickel. The Ni crystallines departed from the fibrous structures and gradually changed to particles through the dissociation of the deposited carbons. The nickel particles were then highly dispersed on the in situ produced carbon, inhibiting the further growth of nickel particle. As a result, the initial fibrous structure morphology of the metallic nickel gradually changed to a pear-like shape.

References

[1] T. Zhang, M.D. Amiridis, Appl. Catal. A 167 (1998) 161.
[2] T.V. Choudhary, C. Sivadinarayana, C.C. Chusuei, A. Klinghoffer, D.W. Goodman, J. Catal. 199 (2001) 9.
[3] R.A. Couttenye, M.H. De Vila, S.L. Suib, J. Catal. 233 (2005) 317.
[4] M.A. Ermakova, D.Yu. Ermakov, G.G. Kuvshinov, Appl. Catal. A 201 (2000) 61.
[5] S. Takenaka, H. Ogihara, I. Yamanaka, K. Otsuka, Appl. Catal. A 217 (2001) 101.
[6] M.A. Ermakova, D.Yu. Ermakov, Catal. Today 77 (2002) 225.
[7] L.B. Avdeeva, O.V. Goncharova, D.I. Kochubey, V.I. Zaikovskii, L.M. Plyasova, B.N. Novgorodov, Sh.K. Shaikhutdinov, Appl. Catal. A 141 (1996) 117.
[8] Sh.K. Shaikhutdinov, L.B. Avdeeva, B.N. Novgorodov, V.I. Zaikovskii, D.I. Kochubey, Catal. Lett. 47 (1997) 35.
[9] M.A. Ermakova, D.Yu. Ermakov, G.C. Kuvshinov, L.M. Plyasova, J. Catal. 187 (1999) 77.
[10] T.V. Reshetenko, L.B. Avdeeva, Z.R. Ismagilov, A.L. Chuvilin, V.A. Ushakov, Appl. Catal. A 247 (2003) 51.
[11] S. Takenaka, S. Kobayashi, H. Ogihara, K. Otsuka, J. Catal. 217 (2003) 79.
[12] J. Li, G. Lu, K. Li, W. Wang, J. Mol. Catal. A 221 (2004) 105.
[13] A. Chambers, T. Nemes, N.M. Rodriguez, R.T.K. Baker, J. Phys. Chem. B 102 (1998) 2251.
[14] K.P. de Jong, J.W. Geus, Catal. Rev.-Sci. Eng. 42 (2000) 481.
[15] K. Otsuka , H. Ogihara, S. Takenaka, Carbon 41 (2003) 223.
[16] T.V. Reshetenko, L.B. Avdeeva, Z.R. Ismagilov, A.L. Chuvilin, V.B. Fenelonov, Catal. Today 102–103 (2005) 115.
[17] L.C. Corrie, S. Jennifer, J.K. Kenneth, Langmuir 18 (2002) 1352.
[18] C. Wang, G. Gau, S. Gau, C. Tang, J. Bi, Catal. Lett. 101 (2005).
[19] J. Liang, Y. Li, Chem. Lett. 32 (2003) 1126.
[20] Z. Liang, Y. Zhu, X. Hu, J. Phys. Chem. B 108 (2004) 3488.

[21] B.D. Cullity, Elements of X-Ray Diffraction, second ed., Addison–Wesley, Menlo Park, CA, 1978.
[22] S.D. Robertson, B.D. Mcnicol, J.H. de Bass, S.C. Kloet, J.W. Jenkins, J. Catal. 37 (1975) 424.
[23] A.G. Boudjahem, S. Monteverdi, M. Mercy, M.M. Bettahar, J. Catal. 221 (2004) 325.
[24] A.G. Boudjahem, S. Monteverdi, M. Mercy, M.M. Bettahar, Catal. Lett. 97 (2004) 177.
[25] T.V. Reshetenko, L.B. Avdeeva, Z.R. Ismagilov, A.L. Chuvilin, Carbon 42 (2004) 143.
[26] P. Wang, E. Tanabe, K. Ito, J. Jia, H. Morioka, T. Shishido, K. Takehira, Appl. Catal. A 231 (2002) 35.
[27] D. Chen, K.O. Christensen, E. Ochoa-Fernández, Z. Yu, B. Tøtdal, N. Latorre, A. Monzón, A. Holmen, J. Catal. 229 (2005) 82.
[28] M.A. Ermakova, D.Yu. Ermakov, L.M. Plyasova, G.C. Kuvshinov, Catal. Lett. 62 (1999) 3.
[29] R.T.K. Baker, Carbon 27 (1989) 315.
[30] J.W. Snoeck, G.F. Froment, M. Fowles, J. Catal. 169 (1997) 240.
[31] K. Sinha, J. Menendez, Phys. Rev. B 41 (1990) 10845.
[32] R.J. Nemanich, S.A. Solin, Phys. Rev. B 20 (1979) 392.
[33] H. Darmstadt, L. Sümmchen, J.M. Ting, U. Roland, S. Kaliaguine, C. Roy, Carbon 35 (1997) 1581.
[34] T. Jawhari, A. Roid, J. Casado, Carbon 33 (1995) 1561.
[35] A. Cuesta, P. Dhamelincourt, J. Laureyns, A. Martinez-Alonso, J.M.D. Tascon, Carbon 32 (1994) 1523.
[36] J.O. Herrera, D.E. Resasco, Chem. Phys. Lett. 376 (2003) 302.
[37] W.E. Alvarez, F. Pompeo, J.E. Herrera, L. Balzano, D.E. Resasco, Chem. Mater. 14 (2002) 1853.